GLOBAL BIOGEOCHEMICAL CYCLES, VOL. 14, NO. 4, PAGES 1353-1370, DECEMBER 2000

Global significance of nitrous-oxide production and transport from oceanic low-oxygen zones: A modeling study

P. Suntharalingam

Earth and Planetary Sciences, Harvard University, Cambridge, Massachusetts

J. L. Sarmiento

Program in Atmospheric and Oceanic Sciences, Princeton University, Princeton, New Jersey

J. R. Toggweiler

Geophysical Fluid Dynamics Laboratory, National Oceanic and Atmospheric Administration, Princeton, New Jersey

Abstract. Recent studies of marine nitrous oxide have focused attention on the suboxic and low-oxygen zones associated with ocean basin eastern boundaries. It has been suggested that complex N_2O cycling mechanisms in these regions may provide a net source to the oceanic interior and a significant portion of the ocean-atmosphere flux. In this study we evaluate the global significance of N_2O formation in these regions. N_2O is treated as a nonconserved tracer in an ocean general circulation model; a simple source function is developed which models N_2O production as a function of organic matter remineralization and local oxygen concentration. Model results are evaluated against both surface and deep observational data sets. The oceanic oxygen minimum zones are predominantly found in the upper water column of tropical latitudes and overlain by regions of strong upwelling in the surface ocean. Simulations of increased N_2O production under low-oxygen conditions indicate that the majority of the N_2O thus formed escapes directly to the atmosphere and is not subject to significant meridional transport. Results indicate that while enhanced N_2O production in these regions cannot be held accountable for the majority of the sea-air flux and interior distribution, it may, however, have significance for the local distribution and provide as much as 25-50% of the global oceanic source.

1. Introduction

Recent studies of marine nitrous oxide have focused attention on the biologically productive regions associated with ocean basin eastern boundaries and characterized by regions of upwelling overlying oxygen-deficient environments. Deep and surface water measurements of N_2O indicate that such environments are the sites of complex N_2O cycling mechanisms where rates of N_2O production and consumption far exceed those observed elsewhere in the ocean [*Codispoti and Christensen*, 1985; *Ward et al.*, 1989; *Codispoti et al.*, 1992]. It has been suggested that these regions may provide a net N_2O source to the oceanic interior and a significant portion of the ocean-atmosphere flux [*Codispoti and Christensen*, 1985; *Codispoti et al.*, 1992; *Naqvi and Noronha*, 1991; *Law and Owens*, 1990].

The prevalent view on the dominant mechanisms responsible for the marine N_2O cycle has changed as information has accumulated on the variety of possible pathways involved in its production and consumption. Since N_2O was known to be an intermediate product in the denitrification of nitrate to gaseous nitrogen, earlier studies of N_2O in the 1970s proposed that this mechanism constituted the primary pathway for marine N_2O formation [*Junge and Hahn*, 1971; *Hahn*, 1974]. Later observations of negative correlations between dissolved oxygen and N_2O, and positive correlations between excess N_2O and oxygen utilization [*Yoshinari*, 1976; *Cohen and Gordon*, 1978; *Elkins et al.*, 1978], along with laboratory evidence indicating that N_2O was also formed as a by-product during bacterially medi-

Paper number 1999GB900100.
0886-6236/00/1999GB900100$12.00

ated nitrification of ammonium to nitrate [*Yoshida and Alexander*, 1970], led to the more recent acceptance of nitrification as the primary source mechanism for marine N_2O production.

The mechanisms of marine N_2O production and consumption are, however, known to exhibit significant complexity at low oxygen levels. N_2O has been observed to be depleted in anoxic waters, a characteristic frequently attributed to the action of denitrifying bacteria which, in the absence of oxygen, utilize N_2O as an oxygen source for respiration [*Elkins et al.*, 1978; *Cline et al.*, 1987; *Naqvi and Noronha*, 1991; *Hashimoto et al.*, 1983; *Cohen and Gordon*, 1978]. Furthermore, elevated levels of N_2O are observed in suboxic waters and at the peripheries of anoxic zones [*Codispoti and Christensen*, 1985; *Ward et al.*, 1989; *Codispoti et al.*, 1992], suggesting enhanced N_2O production in these regions. The mechanisms responsible for such behavior have not, as yet, been fully identified. Recent studies have postulated processes of enhanced nitrification [*Codispoti et al.*, 1989], a hypothesis that is supported by laboratory studies of marine nitrifiers [*Goreau et al.*, 1980]. Alternative mechanisms such as net production by denitrifying bacteria at oxygen levels below 2 μmol/L have also been suggested as the source of this N_2O, based on laboratory evidence on N_2O release from cultures of sedimentary denitrifiers [*Jorgensen et al.*, 1984]. In addition, *Naqvi and Noronha* [1991] have proposed a nitrification-denitrification couple with NO as an intermediate as the dominant mechanism responsible for the observed N_2O distributions in regions of low oxygen.

Codispoti and Christensen [1985] have suggested that rates of N_2O production and consumption can both be high at oxygen levels close to zero ($O_2 \leq 1\%$ saturation), and that the net production is sensitive to small redistributions of oxygen. Figure 1 depicts a schematic form of the proposed relationship between the net N_2O source and local oxygen level which was presented by *Codispoti et al.* [1989] and *Codispoti et al.* [1992]; these studies note that the form of the relationship is supported by measurements made off Peru indicating enhanced N_2O production at sub-oxic levels. If this postulated behavior at low-oxygen concentrations does play an important role in the global N_2O cycle, we can expect to observe significant fluxes to the atmosphere from the low-oxygen zones of the tropics. These low oxygen regions of potential significance for N_2O constitute less than 1.0% of the total oceanic volume, and occur primarily in the northeast tropical Pacific (NETP), the northern Arabian Sea, and the upwelling zone off the coast of Peru.

The purpose of this study is to evaluate the global significance of N_2O formation in such low-oxygen regions and to investigate their potential contribution to global sea-air fluxes and to the oceanic interior distribution. The methodology employs an N_2O source function, which incorporates sensitivity to the local oxygen distribution, embedded in a global ocean general circulation model (OGCM). Model results are evaluated against surface N_2O distributions and sea-air fluxes derived from the measurements of *Weiss et al.* [1992] and also against the deepwater N_2O data of *Butler et al.* [1988]. We stress that the purpose of the study is not to identify specific N_2O cycling mechanisms, but rather to examine the oceanic distribution and sea-air flux generated by a net N_2O source in the ocean's low-oxygen zones.

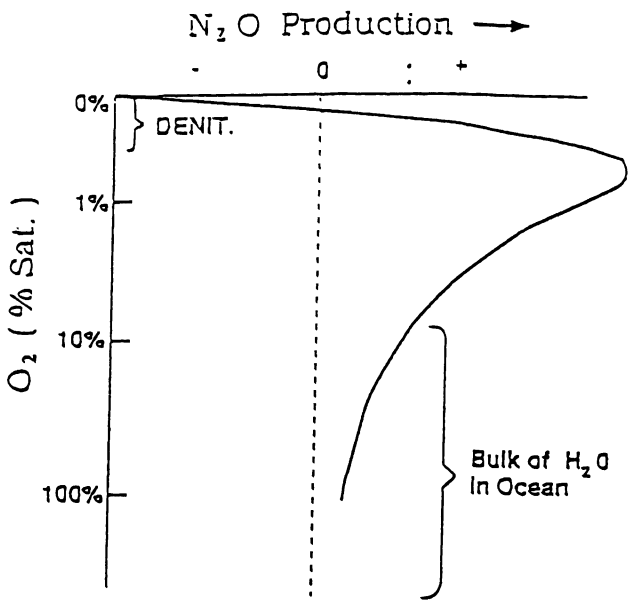

Figure 1. Schematic of suggested relationship between net N_2O production and local oxygen level at low oxygen concentrations in the marine water column (as presented by *Codispoti et al.* [1992]).

2. Model Description

We focus here on a description of the specific formulation of the N_2O source function used for these simulations. Descriptions of the other modeling components employed in the study are summarized in section 2.2; they have also been extensively described by *Toggweiler et al.* [1989a] (ocean circulation model), *Najjar et al.* [1992], *Anderson and Sarmiento* [1995], *Sarmiento et al.* [1995] and *Murnane et al.* [1999] (ocean biogeochemistry model).

2.1. Nitrous Oxide Source Function

N_2O is treated as a nonconserved tracer in an ocean circulation model, where the defining tracer equation can be written as

$$\frac{\partial}{\partial t}[N_2O] + \mathbf{V} \cdot \nabla_H [N_2O] + w \frac{\partial}{\partial z}[N_2O] - A_{HH} \nabla^2 [N_2O] - \frac{\partial}{\partial z}\left(A_{HV} \frac{\partial}{\partial z}[N_2O]\right) = J_{N_2O}. \quad (1)$$

A_{HH} and A_{HV} are horizontal and vertical diffusion coefficients that parameterize mixing by subgrid scale processes. The term J_{N_2O} represents the biological sources and sinks of N_2O.

Nitrate regeneration from ammonium oxidation has been considered unimportant in the euphotic zone, as nitrifying bacteria are believed to be inhibited by light [*Horrigan et al.*, 1981]. We, therefore, assume N_2O production only in the aphotic zone; thus in the euphotic zone,

$$J_{N_2O} = 0 \quad \text{for } z \leq z_e, \tag{2}$$

where z_e represents the depth of the euphotic zone and is 119 m in this configuration of the ocean circulation model (z increasing downward).

In developing an N_2O source function that incorporates sensitivity to the local oxygen level, we rely primarily on the form of the relationship suggested by *Codispoti et al.* [1989] and *Codispoti et al.* [1992] and depicted in Figure 1. The N_2O source function in the aphotic zone is a modified version of the one used for the Base Case scenario of *Suntharalingam* [1997] and *Suntharalingam and Sarmiento* [2000]; in that scenario, N_2O production was modeled as a simple linear function of local oxygen consumption, based on observed correlations between excess N_2O (ΔN_2O, defined as [N_2O - $N_2O_{saturation}$]) and apparent oxygen utilization (AOU). The N_2O source function in this study retains a scalar dependence on oxygen consumption, but also includes a term which incorporates a dependence on local oxygen level, thus allowing for an enhanced N_2O source in low-oxygen regions. It has the form

$$\begin{aligned} N_2O \text{ source} &= \alpha'[O_2 \text{ consumption}] \\ &\quad + \beta f(O_2)[O_2 \text{ consumption}]. \end{aligned} \tag{3}$$

Measures of O_2 consumption are derived from an ocean biogeochemistry model (OBM) previously implemented in the OGCM (see *Murnane et al.* [1999] and discussion of section 2.2.3). Here α' is a scalar multiplier, thus the first term in the above expression is a contribution equivalent to the simple functional form of the Base Case, namely, a constant scalar relationship between N_2O production and oxygen consumption. The second term incorporates the dependence on the oxygen distribution; $f(O_2)$ is a normalized representation of the functional dependence on the oxygen distribution and is parameterized to capture the features of the N_2O source function postulated by *Codispoti et al.* [1992] and *Codispoti et al.* [1989]. The factor β is a scalar multiplier; the basis for the choice of these parameters is discussed below.

In order to parameterize the function $f(O_2)$ representing enhanced N_2O production, we rely on data from *Goreau et al.* [1980], a study which reports laboratory measurements of N_2O yield from marine nitrifiers under conditions of decreasing oxygen concentration. Enhanced N_2O yields, relative to nitrate, are observed as the local oxygen level is lowered; this effect is particularly apparent at oxygen concentrations below 20 μmol/L. The parameterization of $f(O_2)$, therefore, assumes an exponentially increasing dependence of N_2O production with decreasing oxygen level, based on a fit to the data of *Goreau et al.* [1980].

The normalized data from *Goreau et al.* [1980] on relative N_2O/NO_3 production yields and the exponential parameterization selected for model simulations are plotted in Figure 2. Goreau et al.'s study only measures N_2O production rates down to oxygen saturation levels of 2.5%, whereas observed oxygen levels, for example,

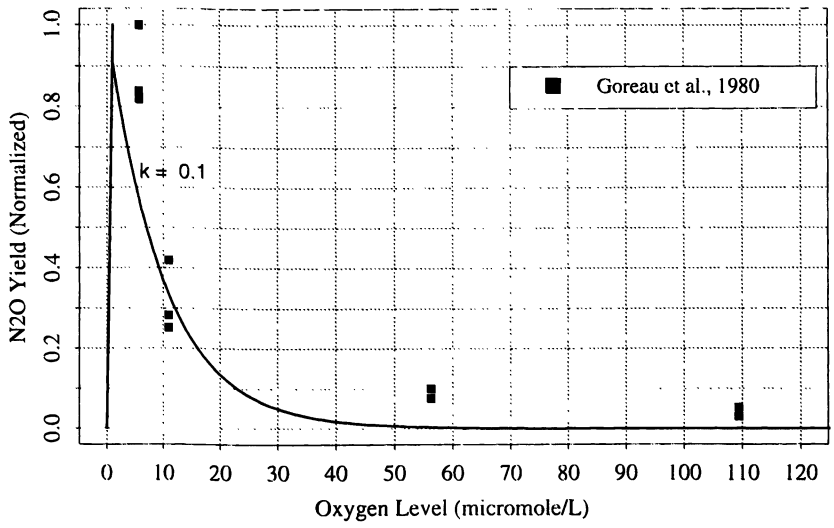

Figure 2. Parametrization of the dependence of N_2O production on local oxygen concentration. The curve depicts the representation used for function $f(O_2)$ of equation 4 and is based on normalized data from *Goreau et al.* [1980] reporting the variation of N_2O yield (relative to nitrite from ammonium oxidation) with of oxygen level.

off the coast of Peru, can fall well below 1.0% [*Elkins et al.*, 1978, *Codispoti et al.*, 1989]. Using the form of the proposed relationship between N_2O production and oxygen level from *Codispoti et al.* [1992] (depicted in Figure 1), we assume for these simulations that the exponential relationship between N_2O yield and decreasing O_2 level also holds in the low-oxygen regime down to 1 μmol/L (i.e., below the lowest oxygen saturation values employed by *Gorcau et al.* [1980]).

Oceanic measurements indicate that the effect of N_2O consumption by denitrification processes becomes significant at oxygen levels close to anoxia (e.g., for $[O_2] <$ 1 μmol/L, [*Prosperie et al.*, 1996]. At oxygen levels of less than 1 μmol/L, therefore, it is assumed that the effect of consumption by denitrification influences the net N_2O source, and production levels drop linearly down to zero. The parameterization of $f(O_2)$ is based on the above assumptions and is given by

$$f(O_2) = [O_2]/O_{max} \quad \text{for } [O_2] < O_{max}$$

$$f(O_2) = \epsilon^{-k([O_2]-O_{max})/O_{max}} \quad \text{for } [O_2] \geq O_{max} \tag{4}$$

$[O_2]$ represents the local oxygen concentration, and O_{max}, the oxygen level at which N_2O production is affected by the onset of denitrification, is set at 1 μmol/L, in accordance with observations from *Prosperie et al.* [1996]. The choice of k is determined by a least squares fit to the *Gorcau et al.* [1980] data and is found to be 0.1. As can be seen in comparison with Figure 1, the structure of the modeled function, $f(O_2)$, captures the main features of Codispoti et al.'s suggested source function for N_2O. In contrast to Codispoti et al.'s figure, we do not explicitly model net N_2O consumption at oxygen levels very close to zero. As discussed below, the model simulations considered in this analysis focus on the net fraction of the global source originating from the low-oxygen zones; hence this simplification in our parameterization for $f(O_2)$ does not affect the larger-scale N_2O distribution outside the oxygen minima.

A further constraint imposed on the modified N_2O source in this study is that the globally integrated source from this parameterization be equal to that of the Base Case of *Suntharalingam* [1997] and *Suntharalingam and Sarmiento* [2000]: the total N_2O source is, therefore, constrained to be equivalent to 3.6 Tg N per year. This constraint was imposed since the focus of the simulations in this study is not to evaluate the magnitude of the oceanic N_2O source, but rather, to investigate the fraction of N_2O transported globally from the low-oxygen regions; this constraint also enables comparison of the resulting N_2O distributions with that of the Base Case simulation. It is implemented by selection of the scalar multiplier β. As can be seen from equation (3), variation of the parameter α' enables partition of the total source between the first and second terms; that is, between the component dependent only on oxygen consumption and the component that includes a dependence on local oxygen level. In the Base Case, the scalar molar ratio α was set to 1.0×10^{-4} in accordance with observations of $\Delta N_2O/AOU$ ratios from a variety of ocean locations [*Suntharalingam and Sarmiento*, 2000]. Therefore, for example, in the modified source function of this study, a value of α' equal to 0.5×10^{-4} allocates half the total N_2O production to the source term independent of oxygen level, and half to the oxygen-dependent source term. By integrating equation (3) over the volume of the aphotic zone, we can calculate β according to the formulation

$$\beta = \frac{\int_x \int_y \int_{z_b}^{z_e} [N_2O \text{ source}]\, dx\, dy\, dz}{\int_x \int_y \int_{z_b}^{z_e} f(O_2)[O_2 \text{ consumption}]\, dx\, dy\, dz} - \frac{\int_x \int_y \int_{z_b}^{z_e} \alpha[O_2 \text{ consumption}]\, dx\, dy\, dz}{\int_x \int_y \int_{z_b}^{z_e} f(O_2)[O_2 \text{ consumption}]\, dx\, dy\, dz}. \tag{5}$$

We reiterate that the formulation for the N_2O source defined in the above section does not attempt to model the specific mechanisms of nitrous oxide turnover in the low-oxygen and anoxic zones; for example, increased production due to a process such as enhanced nitrification, and simultaneous consumption via denitrification as suggested by *Codispoti and Christensen* [1985]. Rather, we plan to examine the net N_2O source originating from these regions and evaluate their potential contribution to the global sea-air flux and the oceanic interior distribution.

We present the results of three separate simulations described below. As noted previously, the global oceanic N_2O source in all three instances is fixed and constrained to be equivalent to 3.6 Tg N per year. The cases considered are as follows: [1] OX1 : The entire source originates from the low-oxygen regions (i.e., α' = 0, and only the oxygen dependent term in equation (3) affects the source function); [2] OX.5 : Half the total source is constrained to originate from the low-oxygen regions, and half follows the parameterization of the Base Case (i.e., $\alpha' = 0.5 \times 10^{-4}$); [3] OX.25 : One quarter of the total source is constrained to originate from the low-oxygen regions, and three quarters follows the parameterization of the Base Case (i.e., $\alpha' = 0.75 \times 10^{-4}$).

In addition, we also compare these simulations against the Base Case scenario of *Suntharalingam and Sarmiento* [2000] and *Suntharalingam* [1997]: [4] Base Case : The source is a function of the oxygen consumption rate alone and has no dependence on oxygen level (i.e., $\alpha' = 1.0 \times 10^{-4}$).

2.2. Other Model Components

2.2.1. Ocean model. The ocean general circulation model (OGCM) employed for the simulations is a version of the Geophysical Fluid Dynamics Labora-

tory's modular ocean model (GFDL-MOM) [*Pacanowski et al.*, 1993]; it is based on the prognostic global model of *Toggweiler et al.* [1989a], with modifications as outlined by *Toggweiler and Samuels* [1993]. The model is a nonseasonal global ocean GCM of horizontal resolution 4.5° latitude by 3.75° longitude; it has 12 levels in the vertical and a maximum depth of 5000 m. Mixing by subgrid scale processes is parameterized by horizontal and vertical diffusion coefficients. The model is forced at the surface by the annual mean wind stresses of *Hellerman and Rosenstein* [1983], and surface forcing heat and freshwater fluxes are calculated by restoring model potential temperature and salinity to the annual climatological averages of *Levitus* [1982].

2.2.2. Gas Exchange. The flux of N_2O across the air-sea interface is calculated as a product of the gas transfer velocity k_w and the concentration difference across the interface; thus

$$\mathrm{Flux}_{N_2O} = (1 - f_i)k_w([N_2O]_{atm} - [N_2O]_{ocean}). \quad (6)$$

where f_i represents the fraction of the local ocean surface under ice cover. The gas transfer velocity, k_w, is influenced in a complex manner by interfacial turbulence, the kinematic viscosity of the water μ, and the diffusion coefficient of the gas D. It is often parameterized as a function of wind speed U, and the Schmidt number Sc, which represents the dependence of k_w on the latter two terms (i.e., $Sc = \mu/D$). The gas transfer velocity employed for the simulations in this study is the formulation of *Wanninkhof* [1992],

$$k_w(U, Sc) = 0.39U^2\left(\frac{Sc}{660}\right)^{-0.5}. \quad (7)$$

Equation (7) is evaluated using annual-mean wind speeds from the observational analysis of *Esbensen and Kushnir* [1981] gridded to the OGCM resolution of 4.5° latitude by 3.75° longitude.

2.2.3. Ocean biogeochemistry model. The ocean biogeochemistry model (OBM) is a modified version of the phosphate-based model of *Najjar et al.* [1992]; details of its implementation in the OGCM are discussed by *Murnane et al.* [1999] and *Sarmiento et al.* [1995]. Simulated tracers involved in the model's new production and remineralization cycle include phosphate, dissolved organic phosphorus (DOP), and oxygen. New production of organic matter in the model's euphotic zone is simulated by restoring phosphate levels to the observations of *Najjar et al.* [1992]. Since the development and validation of the OBM have been extensively outlined in the above studies as well as by *Anderson and Sarmiento* [1995], we do not further describe it here. We will, however, discuss the accompanying oxygen simulation in more detail, as its distribution directly affects N_2O production in this set of simulations. As with the other biological tracers involved in the OBM, oxygen is transported by the OGCM advection, diffusion, and convection fields, and subject to biological sources and sinks, and gas exchange processes at the model's air-sea interface.

Oxygen is produced in the euphotic zone in proportion to organic phosphorus production via an oxygen to phosphorus Redfield ratio of 170:1 [*Anderson and Sarmiento*, 1994]. Oxygen consumption in the aphotic zone is governed by linking it to organic phosphorus remineralization again with the same oxygen to phosphorus Redfield ratio. It is allowed to exchange across the air-sea interface with an atmospheric reservoir of constant concentration of 285 ppmv. The air-sea flux of oxygen is parameterized as

$$\mathrm{Flux}_{O_2} = (1 - f_i)k_w([O_2]_{atm} - [O_2]_{ocean}). \quad (8)$$

As for N_2O, the parameterization employed for the gas exchange coefficient k_w in the oxygen simulations is the wind speed dependent formulation from *Wanninkhof* [1992]. $[O_2]_{atm}$ represents the equilibrium concentration of dissolved oxygen in seawater in contact with moist air and is computed using the temperature- and salinity-dependent formulation of *Benson and Krause* [1984]. Further details of the oxygen distribution employed for the N_2O simulations are given by *Anderson and Sarmiento* [1995], *Najjar* [1990], and *Suntharalingam and Sarmiento* [2000].

3. Discussion and Results

3.1. Low Oxygen Regions

Before presenting the results of the cases run, we first discuss the locations of the low-oxygen regions, since these are also the sites of the highest N_2O production in these simulations. In this section we also note that certain characteristics of the coarse grid annual mean OGCM result in some unrealistic aspects of the modeled oxygen distribution and have consequent implications for the N_2O source distribution.

3.1.1. Locations of the low-oxygen regions. The low-oxygen regions, of potential significance to the N_2O distribution, occur primarily north and south of the equator in the eastern tropical Pacific, and the northwest Arabian Sea [*Codispoti et al.*, 1992; *Naqvi and Noronha*, 1991]. As noted by *Codispoti et al.* [1992], the regions of significance for N_2O production are not limited to the narrow coastal upwelling zones, but encompass the deep intense oxygen minima that exist over scales of hundreds of kilometers.

Figure 3 maps those regions where the modeled oxygen distribution in the water column falls below 20 μmol/L at a depth of almost 500 m. Figure 4 depicts the location of the model's oxygen minimum in the water column at a meridional section in the eastern Pacific (120°W). As can be seen, the model's low oxygen

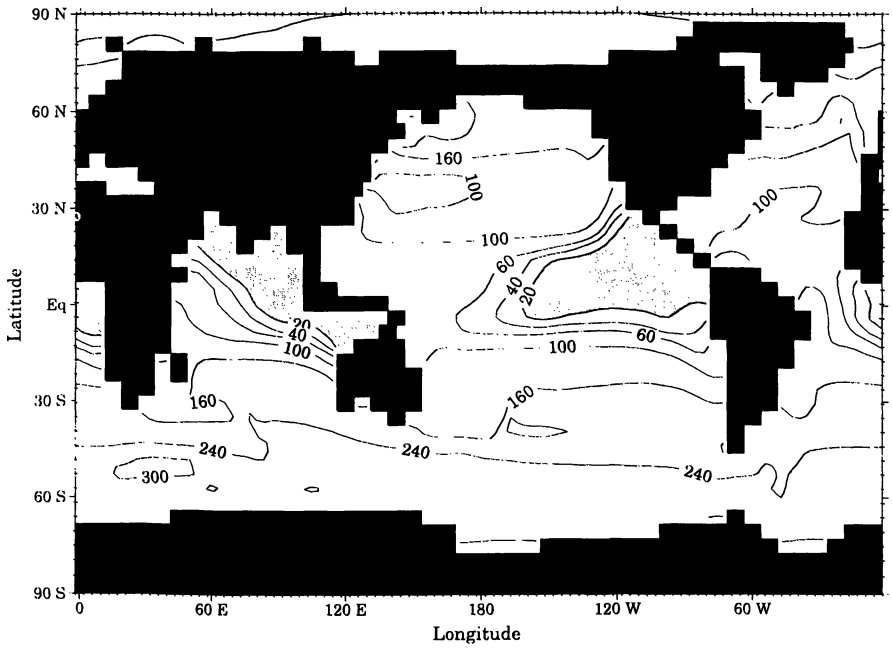

Figure 3. Low-oxygen regions in the ocean circulation model. Values are depicted for model level 5, which has a midpoint depth of 483 m, and are in units of μmol/L. Shading indicates regions where the oxygen concentration falls below 20 μmol/L.

zones are situated in the low latitudes (between 20°S and 20°N), and in the upper water column (at depths of 300 m to 1200 m).

In a study on the position of the oceanic oxygen minimum, *Wyrtki* [1962, p.21] noted that while biological consumption of oxygen is the primary and necessary condition for the existence of the O_2 minimum, its position is also strongly influenced by local circulation; that is, "the minimum tends to develop in layers of minimum advection of oxygen, which are closely related to layers of minimum horizonal movement ...The large bodies of extremely low O_2 content are formed on the eastern sides of the ocean in sub-tropical regions where horizontal circulation is weak and where vertical ascending movements prevail."

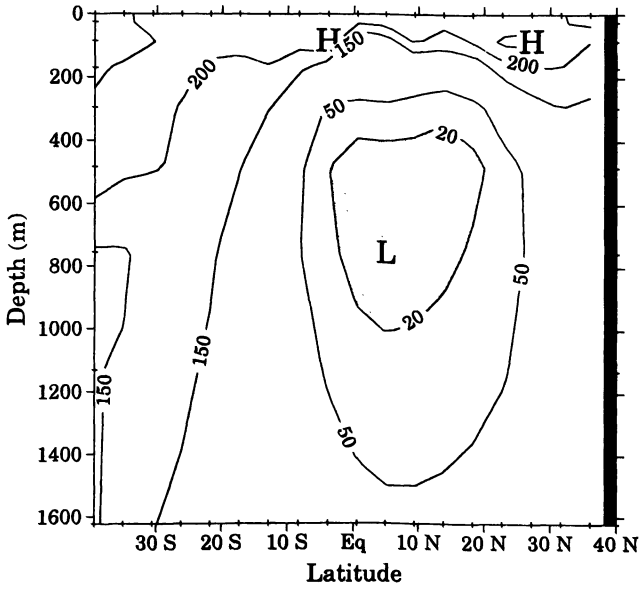

Figure 4. Location of modeled oxygen minimum in the water column at 120°W. Contours denote O_2 concentrations in μmol/L.

Toggweiler et al. [1989a, 1991] presented analyses of the upper ocean vertical velocity field in the OGCM. As is seen in these studies, the regions most closely associated with the oxygen minima, and consequently with the most intense N_2O production, are characterized by strong vertical upwelling. As will be discussed later, the circulation characteristics associated with the oxygen minima also conspire to allow the majority of N_2O formed in such locations to escape to the atmosphere without being subject to significant lateral advection.

3.1.2. Circulation model influences on the low-oxygen regions. Observational evidence indicates that the anoxic and suboxic regions in the eastern Pacific, namely, the NETP off the coast of Central America, and the upwelling region off Peru, are separated by a tongue of more oxygenated water advected eastward by the Equatorial Undercurrent at depths of 100 to 300 m [*Tschuyia*, 1968]. As noted by *Toggweiler et al.* [1991], a characteristic of the coarse grid version of the circulation model used in these simulations is that the flow speeds and volumes of intense currents

are not well reproduced, due to the high imposed viscosity necessary for numerical stability. In particular, the Equatorial Undercurrent only achieves up to 25% of maximum estimated speeds of 100 m/s [*Wyrtki*, 1981]. A consequence of this for the modeled oxygen distribution in the eastern tropical Pacific is that the two distinct oxygen minimum zones north and south of the equator seen in the observations are not as well delineated, as insufficient higher-oxygen water is transported eastward by the weak modeled Undercurrent.

In the northern Indian Ocean the Arabian Sea is observed to display high rates of primary productivity, and its upwelling zones are estimated to provide a significant source of N_2O to the atmosphere [*Naqvi and Noronha*, 1991; *Law and Owens*, 1990]. Owing to a combination of high productivity and poor ventilation, subsurface oxygen levels drop close to zero in the northwest Arabian Sea; it is known to be a site of active denitrification, as well as a location where elevated N_2O levels have been measured at the boundaries of suboxic zones [*Naqvi and Noronha*, 1991; *Naqvi et al.*, 1996]. Much of the enhanced productivity and high-N_2O efflux from upwelling zones are, however, dependent on the wind-driven monsoonal circulation, the effect of which is more apparent in the Arabian Sea than in the neighboring more stably stratified Bay of Bengal. The OGCM used for this set of simulations is, however, nonseasonal and forced at the surface by annually averaged wind stresses. A consequence in the North Indian Ocean is that the monsoonal circulation is not well reproduced. The seasonal intense upwelling in the north west Arabian Sea is not distinct; instead, the climatologically averaged wind stresses drive a weak diffuse upwelling over much of the northern Indian Ocean [*Toggweiler et al.*, 1989a]. Although oxygen levels fall below 1 μmol/L in the Arabian Sea, they are also low in the Bay of Bengal (which is not observed to be a site of active dentrification [*Rao et al.*, 1994]). Furthermore, the closing of the Indonesian Straits in this configuration of the OGCM [*Toggweiler and Samuels*, 1993] cuts off a supply of oxygenated water to the upper levels of the northeast Indian Ocean and results in low oxygen concentrations in these regions as well.

In the Indian Ocean, therefore, and to a lesser exent in the Pacific Ocean, the model's low-oxygen zones are somewhat more extensive than in reality; for example, a comparison of the fraction of the global oceanic volume contained in waters of oxygen content less than 20 μmol/L yields 1.2% for the OGCM in comparison to $\leq$ 1.0% as calculated from the *Levitus et al.* [1994] atlas of oceanic oxygen concentrations. A consequence for the simulations considered in this study is that the spatial extent of the low-oxygen N_2O source regions is also more widespread than predicted by the observations,

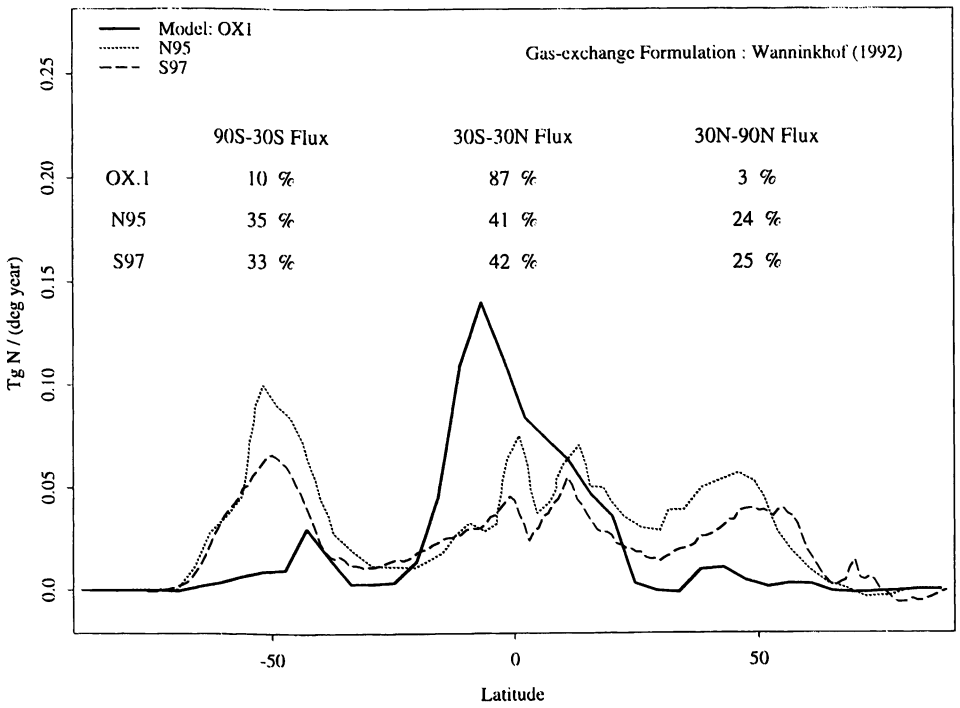

Figure 5a. Zonally integrated sea-air N_2O flux from OX1, and comparison with observation-based estimates from *Nevison et al.* [1995] (N95, global flux = 5.2 Tg N per year) and *Suntharalingam* [1997] (S97, global flux = 4.0 Tg N per year). The global flux for all model simulations is 3.6 Tg N per year.

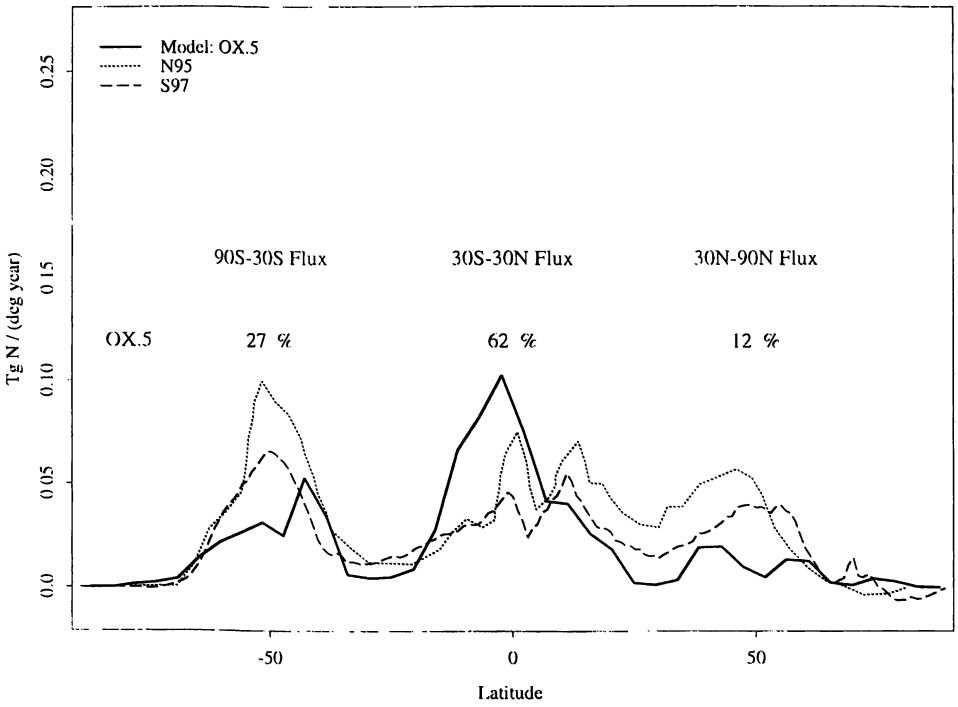

Figure 5b. Zonally integrated sea-air N_2O flux from OX.5, and comparison with observation-based estimates from *Nevison et al.* [1995] (N95) and *Suntharalingam* [1997] (S97).

thus leading to model overestimates of N_2O formation and transport from these regions. The implications for our study are further discussed in section 3.2.

3.2. Zonally Integrated Sea-Air Fluxes

Figures 5a-5c depict the zonally integrated ocean to atmosphere N_2O fluxes for each of the three OX simulations and comparison with two separate distributions derived from observational surface N_2O data, namely, N95 [*Nevison et al.*, 1995] and S97 [*Suntharalingam*, 1997]. Figure 5d illustrates the flux distribution from the Base Case results of *Suntharalingam and Sarmiento* [2000]. Table 1 lists the net sea-air fluxes from the latitude bands 90°S - 30°S, 30°S - 30°N, and 30°N - 90°N for both model simulations and observation-based distributions; also included are model results on the fractions of the total marine N_2O source produced within these latitude belts and the net northward oceanic N_2O transport across the 30°S and 30°N latitude boundaries.

The observation-based flux distributions of S97 and N95 both rely primarily on the *Weiss et al.* [1992] database for derivation of the air-sea partial pressure difference (ΔpN_2O). Methods of interpolation, however, differ between the two studies and are discussed further by *Suntharalingam* [1997]. The estimates shown employ the gas exchange formulation of *Wanninkhof* [1992], as do the model simulations. It should be noted that the total global fluxes derived from the observation-based distributions differ from each other as well as from the model simulations; that is, global fluxes per year of 4.0 Tg N (S97), 5.2 Tg N (N95) and 3.6 Tg N (model simulations). For this reason it is more appropriate to compare the modeled and observed flux distributions on a percentage basis across the three latitude zones.

As seen in Figure 5, the observationally based flux distributions are distinctly trimodal with elevated N_2O fluxes in the high latitudes and the tropics; the minima centered at 30°S and 30°N correspond to the oligotrophic subtropical gyres that contribute little to the global N_2O flux. Of the OX simulations the one that is closest to the structure and relative magnitudes of the observed flux pattern is OX.25; that is, the case which represents a global contribution of 25% of the enhanced N_2O source from the low-oxygen regions. In contrast, simulation OX1, which assigns the entire oceanic N_2O source to the low-oxygen regions of the tropics, produces a latitudinal flux distribution dominated by a single equatorial maximum. Of the 3.6 Tg N of N_2O per year produced in the equatorial latitudes, the majority (87%) effluxes to the atmosphere in the same latitudinal zone, with only 0.3 Tg N and 0.1 Tg N being transported south and north, respectively, to the higher latitudes. In contrast, the observational flux estimates predict that only 41-42% of the net sea-air flux effluxes in the equatorial zone. The OX1 simulation, admittedly, represents an extreme case, but does serve

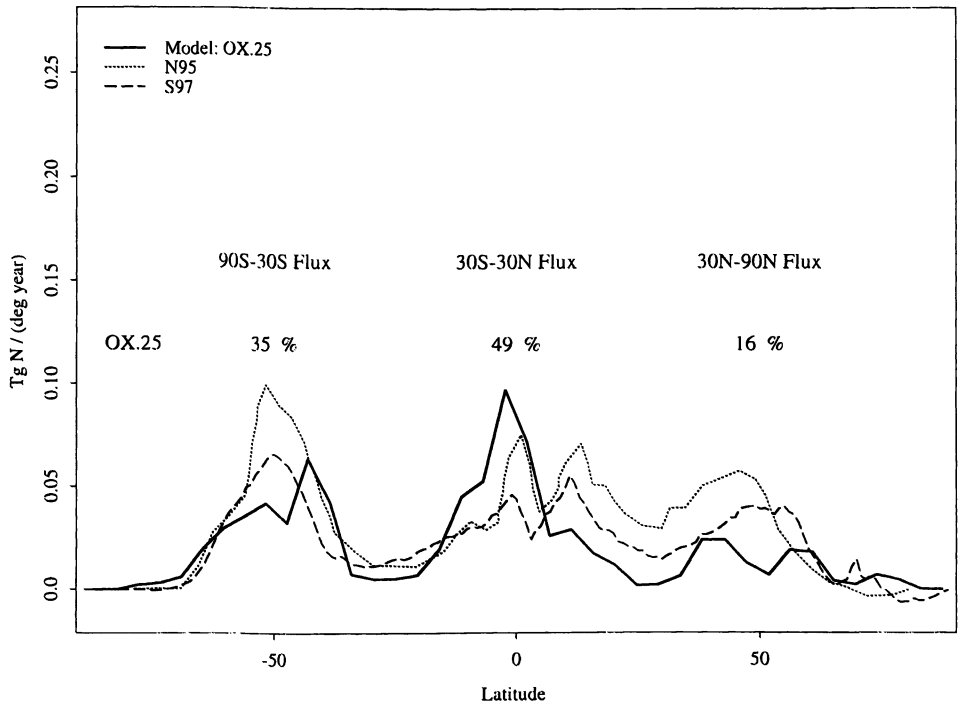

Figure 5c. Zonally integrated sea-air N_2O flux from OX.25, and comparison with observation-based estimates from *Nevison et al.* [1995] (N95) and *Suntharalingam* [1997] (S97).

to demonstrate that for the source location in question, characterized by equatorially convergent and upwelling circulation patterns and situated in the upper ocean, most of the in situ source escapes directly to the atmosphere without entering the deeper circulation and being transported to the higher latitudes. The deep meridional oceanic transport of N_2O in these simulations will be discussed in more detail in section 3.4.

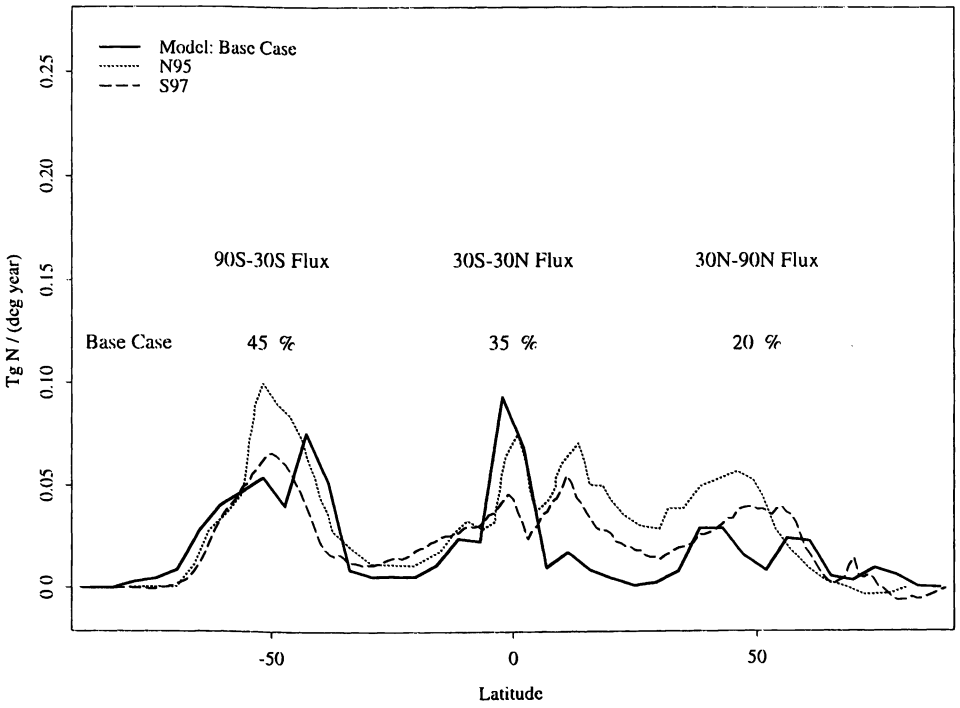

Figure 5d. Zonally integrated sea-air N_2O flux from the Base Case, and comparison with observation-based estimates from *Nevison et al.* [1995] (N95) and *Suntharalingam* [1997] (S97).

Table 1. Summary of Oceanic N_2O Source and Sea-Air Flux by Latitude Belt, and the Net Meridional Transport at the 30°S and 30°N Boundaries.

Latitude Belt	Source Tg N/yr	Flux Tg N/yr	Meridional N_2O Transport at Boundary Tg N/yr	
			30°S	30°N
Model Simulations				
OX1				
90°S - 30°S	0.0 (0%)	0.3 (10%)	-0.3	
30°S - 30°N	3.6 (100%)	3.2 (87%)		
30°N - 90°N	0.0 (0%)	0.1 (3%)		0.1
OX.5				
90°S - 30°S	0.65 (18%)	1.0 (27%)	-0.35	
30°S - 30°N	2.65 (74%)	2.2 (62%)		
30°N - 90°N	0.30 (8%)	0.4 (12%)		0.1
OX.25				
90°S - 30°S	1.0 (28%)	1.35 (35%)	-0.35	
30°S - 30°N	2.2 (61%)	1.75 (49%)		
30°N - 90°N	0.4 (11%)	0.50 (16%)		0.1
Base Case				
90°S - 30°S	1.28 (35%)	1.64 (45%)	-0.36	
30°S - 30°N	1.75 (48%)	1.28 (35%)		
30°N - 90°N	0.62 (17%)	0.73 (20%)		0.11
Observation-based Estimates				
S97				
90°S - 30°S		1.31 (33%)		
30°S - 30°N		1.66 (42%)		
30°N - 90°N		0.99 (25%)		
N95				
90°S - 30°S		1.82 (35%)		
30°S - 30°N		2.13 (41%)		
30°N - 90°N		1.25 (24%)		

Included for comparison with the model simulations are the observation-based flux estimates from *Suntharalingam* [1997] (S95) and *Nevison et al.* [1995] (N95). Positive values of meridional transport indicate net northward flow.

As the dependence of the source function on the low-oxygen regions decreases, and as the role of N_2O production based solely on oxygen consumption increases (i.e., as the first term in equation (3) assumes more importance relative to the second), a trimodal flux distribution with latitude begins to emerge. OX.5, for example, allows half the total source to be produced in regions outside the low-oxygen zones of the tropics; consequently, the flux distribution in the higher latitudes begins to mirror that of the Base Case (Figure 5d), which predicts high fluxes from these regions as well as from the tropics. The Base Case scenario, therefore, constitutes a limiting case of this progression; that is, there is no dependence of the N_2O source on the low-oxygen zones, and hence, $\beta = 0$ in equation (3). The inability of the OX1 simulation to reproduce the structure of the observed distribution suggests that the majority of the ocean-atmosphere flux in high latitudes must be formed in situ, and not advected from the low-latitude oxygen minimum regions.

As noted in section 3.1.2, the OGCM circulation characteristics result in an overestimate of the spatial extent of the low-oxygen regions and hence of the N_2O source locations in the tropics. A more accurate model representation of these regions is likely to further constrain the N_2O source regions to equatorial upwelling zones and hence lead to increased N_2O efflux from a more limited extent than in the current simulations. The equatorial flux maxima of Figures 5a-5c, for example, are likely to become more sharply delineated and less diffused over the 30°S - 30°N tropical band. Thus an even smaller proportion of N_2O formed in the tropics is

likely to be subject to transport to the high latitudes. A more accurate constraint on the limit of the low-oxygen zones is likely to result in an even greater proportion of the modeled N_2O source effluxing in the tropical latitude band.

Some caveats must, however, also be added on the coverage of the underlying observational database used in the above comparison. Both observational studies predict significant fluxes (33-35%) from the southern high latitudes. Both studies are predominantly based on the surface ocean N_2O database of *Weiss et al.* [1992], which is sparse in the Southern Ocean. There is, therefore, a margin of uncertainty associated with the observed flux estimates from this region. Furthermore, although the Base Case model result for these latitudes (45% of the global sea-air flux) is higher than the observational fluxes, this may in part be due to regions of anomalous model convection, leading to overestimates of productivity and hence of N_2O production in parts of the Southern Ocean [*Najjar*, 1990; *Suntharalingam and Sarmiento*, 2000]. The Base Case fluxes from the high southern latitudes should, therefore, also be viewed with caution.

In addition, in the low latitudes, although the *Weiss et al.* [1992] database has reasonable coverage in the NETP, there is sparse coverage of the region off Peru and a single cruise track in the Arabian Sea which misses the southwest monsoon. *Bange et al.* [1996], in a study on N_2O fluxes from estuaries and coastal upwelling zones, noted that although such areas have often been ignored in a global accounting of oceanic N_2O fluxes, the extremely high supersaturations measured here could potentially outweigh their small areal extent and yield significant contributions to the global flux. We note, therefore, that a more comprehensive coverage of such regions of potential significance to the N_2O distribution is desirable if we are to have more confidence in the observed flux estimates against which we compare the model. In view of such uncertainties in both the model and observations, we conclude that on the basis of the surface flux analysis about 25%, and possibly up to 50%, of global oceanic N_2O could originate in these low-latitude low oxygen regions.

3.3. Depth Averages of ΔN_2O

In evaluating the modeled distributions at depth, we employ the quantities apparent oxygen utilization (AOU) and excess N_2O (defined as $\Delta N_2O = [N_2O - N_2O_{saturation}]$). Use of these respective deficit and surplus quantities, which represent the predominantly biological contributions to the tracer distributions, allows us to circumvent errors in the oxygen and N_2O fields introduced by model temperature problems in the thermocline [*Najjar et al.*, 1992; *Anderson and Sarmiento*, 1995; *Suntharalingam and Sarmiento*, 2000].

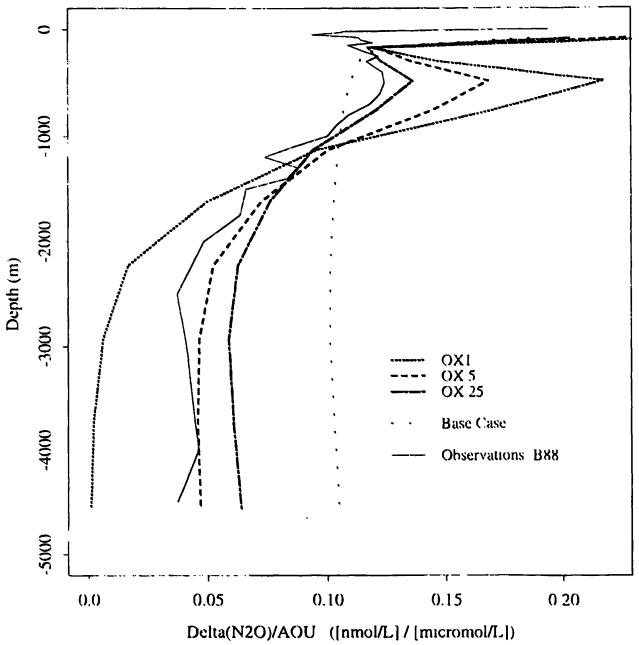

Figure 6. $\Delta N_2O/AOU$ variations with depth for the three OX simulations, and comparison with the Base Case and observations of *Butler et al.* [1988] (B88).

In evaluating the deep distribution we compare the averaged depth profiles of $\Delta N_2O/AOU$ ratios obtained from these simulations with observed values. Figure 6 depicts the variation with depth of the modeled ratios of $\Delta N_2O/AOU$ against the observations from the Soviet-American Gas and Aerosol Experiment (SAGA) 2 cruises of *Butler et al.* [1988] and the result obtained for the Base Case simulation. (Recall that the Base Case assumes a constant molar ratio of 0.1×10^{-3} between N_2O production and oxygen consumption; as was noted by *Suntharalingam and Sarmiento* [2000] this simple parameterization is not successful in reproducing the observed variations of $\Delta N_2O/AOU$ at depth.) Figure 6 indicates, however, that inclusion of the dependence on oxygen level in the source function results in a better fit to the data, for all three oxygen-dependent simulations, in comparison to the Base Case, that is, high $\Delta N_2O/AOU$ ratios ($\geq 0.1 \times 10^{-3}$) at the surface and low values at depth ($\leq 0.07 \times 10^{-3}$). Simulation OX.25 gives the closest fit to the data in the critical upper oceanic regions where the majority of the N_2O is formed, with a maximum of 0.14×10^{-3} at a depth of 500 m, in comparison to a maximum level of about 0.12×10^{-3} for the *Butler et al.* [1988] data at the same depth. The OX.5 and OX1 simulations yield much higher $\Delta N_2O/AOU$ ratios at this depth of greater than 0.18×10^{-3} and 0.2×10^{-3} respectively.

In the deep ocean the best fit to the data is achieved by OX.5, which comes close to the *Butler et al.* [1988]

values of about 0.05 x 10^{-3}. OX1 yields deep values of $\Delta N_2O/AOU$ close to zero, since no N_2O is produced in the deep ocean in this simulation. The OX.25 simulation has a $\Delta N_2O/AOU$ ratio of about 0.07 x 10^{-3} at depth, that is, higher than the observed values. The better fit of OX.5 to the data in the deep ocean is unsurprising, as the coefficient α' in equation (3) was set to 0.05 x 10^{-3} for this scenario. Note that α', which defines the ratio of N_2O production to oxygen consumption outside the low-oxygen regions, is the dominant influence on the $\Delta N_2O/AOU$ ratios in the deep ocean. In comparison, OX.25, which allocates three quarters of the total source to the non-low-oxygen regions, has an α' value of 0.075 x 10^{-3}, which is responsible for its higher $\Delta N_2O/AOU$ levels in the deep ocean.

The Base Case employs an α' value of 0.1 x 10^{-3} throughout the global ocean and hence does not reproduce the decrease with depth in the $\Delta N_2O/AOU$ ratios apparent in the SAGA 2 data. As noted by *Suntharalingam and Sarmiento* [2000] and *Suntharalingam* [1997] a better fit to the data is obtained if some form of dependence on depth is incorporated into the N_2O source function, for example, allowing the ratio of N_2O production to oxygen consumption to decrease with depth, thus concentrating a greater proportion of the total source higher up in the water column. As we see here, the OX simulations of this study imply that a better fit to the deep water data, in comparison to the Base Case, may also be obtained by introducing a dependence on the low-oxygen regions into the source function. Since these regions are located in the upper ocean at depths above 1000 m, the effect on the vertical N_2O source distribution is comparable to shifting a significant fraction of the total source into the upper water column. Table 2 summarizes the variation with depth of the N_2O source for the three OX simulations and the Base Case. As can be seen, in all OX cases, less N_2O is produced at depths below 1000 m than in the Base Case; for example, the OX.5 case which best matches the observational data at depth has a deep N_2O source just over half that of the Base Case (9% of the global source as compared to 16% for the Base Case). However, the good match between OX.5 and the observations at depth has a relatively small effect on the surface fluxes and distribution, as these are driven by the upper ocean N_2O source; in all scenarios the majority of marine N_2O is produced at depths above 500 m, in keeping with locations of the maxima in distributions of organic matter remineralization and oxygen consumption, and also with the local oxygen minimum zones.

Table 2. Distribution of the Modeled Global N_2O Source With Depth: OX Simulations and Base Case

Simulation	Percentage of Global Source	
	Above 1000 m	Below 1000 m
OX1	98%	2%
OX.5	91%	9%
OX.25	87%	13%
Base Case	84%	16%

Table 3. Global Oceanic N_2O Inventories: Model Simulations and IPCC 1990 Estimate

Simulation	Global Oceanic N_2O Inventory Tg N
OX1	860
OX.5	966
OX.25	990
Base Case	1080
IPCC 1990 estimate	900-1100

The 1990 Intergovernmental Panel on Climate Change (IPCC) estimate is based on data reported in *Butler et al.* [1988]

A further effect of this concentration of the N_2O source in the upper reaches of the water column in the OX simulations is that a larger fraction of the total source is formed in the tropical upwelling zones (than in the Base Case); this N_2O is then vented directly to the atmosphere and not mixed into the deep ocean. This results in the total inventory of N_2O being lower for the three OX simulations of this study than for the Base Case, as summarized by Table 3. The simulation with the highest proportion of the total source in the upper ocean, namely OX1, accumulates the smallest inventory of 860 Tg N, in comparison to OX.25 with 990 Tg N and the Base Case with 1080 Tg N. Apart from OX1 the global inventories of all simulations lie within the bounds of the 1990 Intergovernmental Panel on Climate Change (IPCC) estimate of 900 - 1100 Tg N [*Houghton et al.*, 1990].

3.4. Meridional Oceanic Transport of N_2O

As discussed in section 3.2 and demonstrated by Table 1, the majority of the N_2O formed in the tropics in the OX simulations effluxes to the atmosphere in the latitude zone of formation. The remainder is transported meridionally to higher latitudes, and we now examine the transport of this latter component; in the OX1 simulation, for example, it is this component that determines the net sea-air flux outside the tropics.

Figures 7a-7c depict the variation with depth of the zonally integrated meridional flow of N_2O across the 30°S and 30°N latitude boundaries for each of the OX simulations (positive values indicate northward flow).

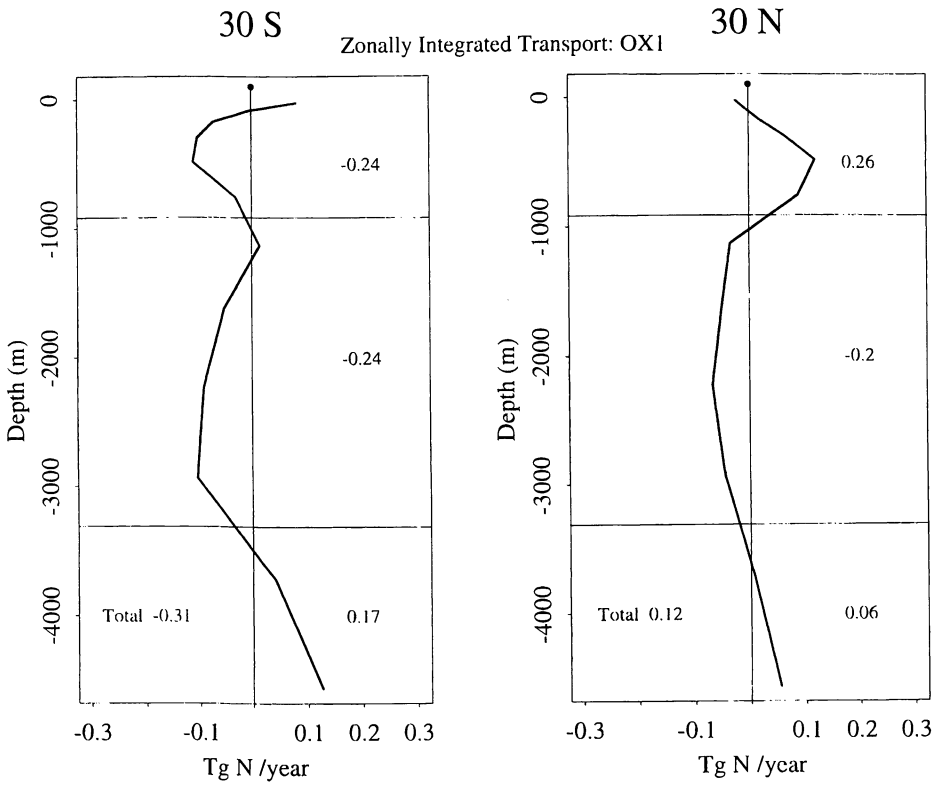

Figure 7a. Simulation OX1: depth variation of the zonally integrated meridional transport at 30°S and 30°N. The numbers in the right-hand half of each plot indicate the net transport at the partitioned depths, that is, 0-914 m, 914-3311 m, and 3311-5000 m. The total in the left-hand half of each plot gives the net meridional transport across the latitude belt. Positive values indicate northward transport.

First, we consider the most extreme case, OX1, in which the entire source originates in the tropical belt between 30°S and 30°N. The net annual outflows across the southern and northern boundaries of this zone are 0.3 Tg N and 0.1 Tg N per year, respectively, and represent the portion of the total N_2O source transported poleward and not effluxed to the atmosphere in the tropics. Figure 7a indicates poleward transports of 0.24 Tg N and 0.26 Tg N across 30°S and 30°N in the upper 1000 m of the ocean, suggesting that the majority of the polewards transport of the "low oxygen" N_2O source occurs in this depth range.

The deep ocean transport consists of net northward bottom transport at depths of 3500 - 5000 m and a net southward return transport at intermediate depths of 1000 - 3500 m. Figures 7b and 7c indicate that OX.5 and OX.25 demonstrate similar overall patterns of oceanic N_2O transport; however, examination of Table 1 suggests that the net outflows across 30°S and 30°N are slightly larger for OX.5 and OX.25 than for OX1 (e.g., total outflows of 0.45 Tg N per year for the former scenarios, in comparison to 0.4 Tg N per year for OX1). This result is a little unexpected since the magnitude of the total source originating in the 30°S - 30°N latitude belt is much higher for OX1 (3.6 Tg N per year) than for the other two scenarios (2.65 Tg N and 2.2 Tg N for OX.5 and OX.25, respectively). It can, however, be explained by considering the variation of the locations of the N_2O source among the simulations. The OX1 simulation constrains the entire source to be produced in the low-oxygen regions predominantly above 1000 m, and often in regions of strong vertical upwelling, whereas for the two other simulations we also model an N_2O source accompanying remineralization outside these low-oxygen zones (i.e., via the first term of equation (3)). OX.5 and OX.25, therefore, produce a fraction of the total source at deeper levels and in regions where it is not as easily vented to the atmosphere; the N_2O thus formed is more likely to be transported laterally by the deeper circulation resulting in a small increase in net poleward transport in comparison to OX1.

In evaluating N_2O transport from tropical source regions as done in this study, it is necessary to assess the accuracy of the ocean model's meridional transport; if, for example, poleward flow is greater in reality, would

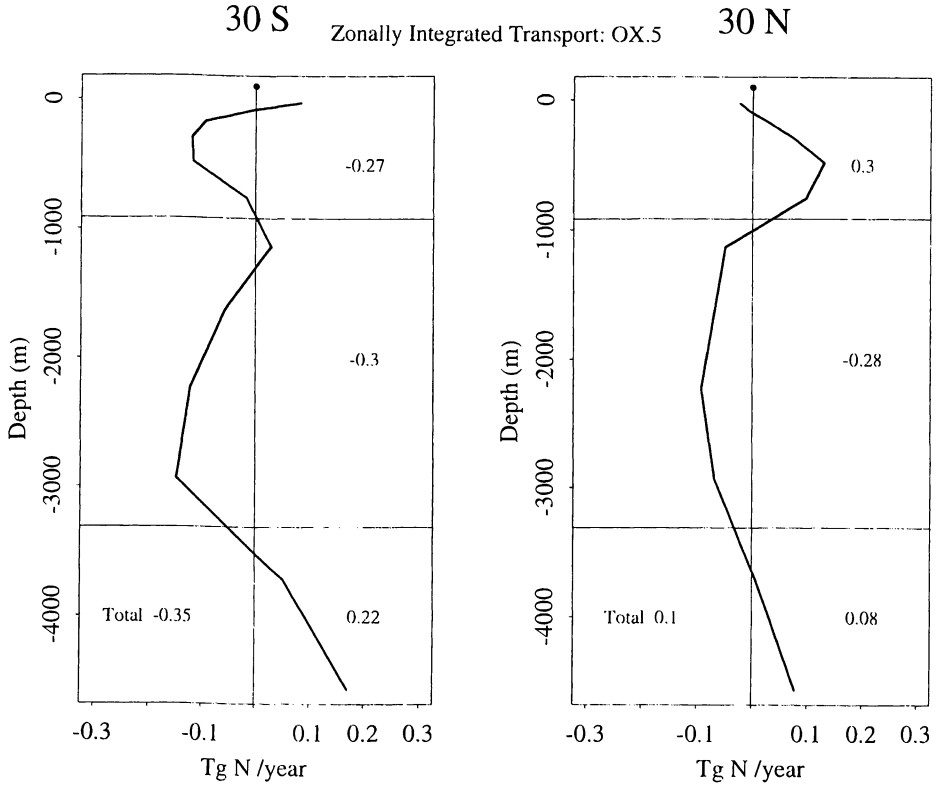

Figure 7b. Simulation OX.5: depth variation of the zonally integrated meridional transport at 30°S and 30°N.

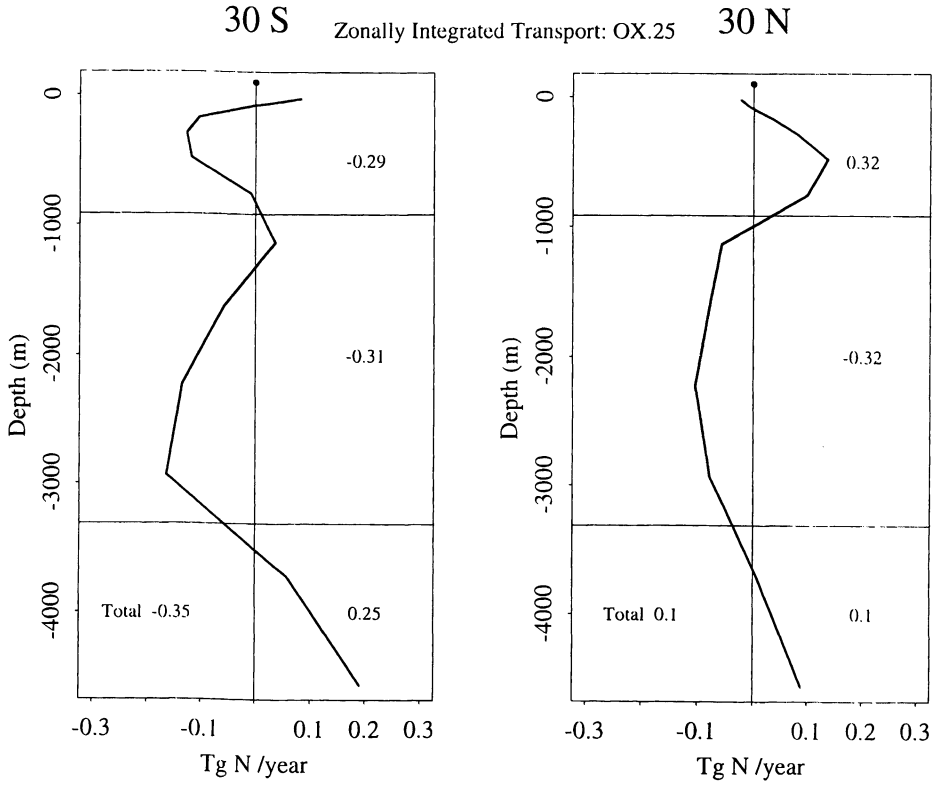

Figure 7c. Simulation OX.25: depth variation of the zonally integrated meridional transport at 30°S and 30°N.

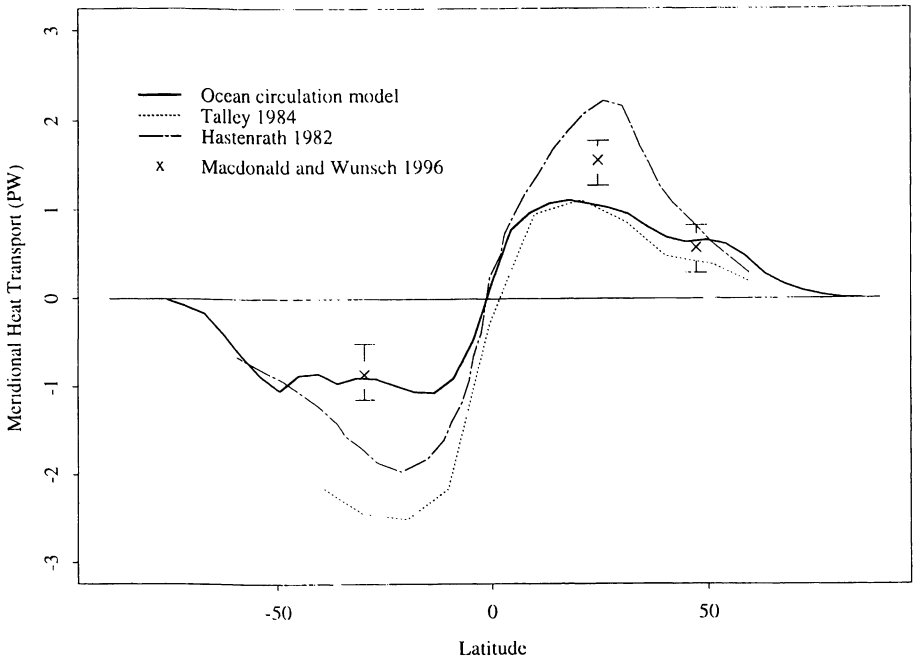

Figure 8. Global meridional heat transport by the ocean circulation model and comparison with the estimates of *Macdonald and Wunsch* [1996], *Talley* [1984], and *Hastenrath* [1982]. Positive values indicate northward transport.

an improved model circulation allow sufficient N_2O to be transported from the tropics to high latitudes so as to better match the observational sea-air flux for even the more extreme OX scenarios ? In a study of the ocean carbon cycle using this OGCM, *Murnane et al.* [1999] indicated that the ocean model does not produce the net southward interhemispheric flow of carbon postulated by the studies of *Broecker and Peng* [1992] and *Keeling and Peng* [1995]. Lacking data on meridional transport of N_2O in the global ocean, we compare instead model meridional heat transports to observationally based estimates. Although heat is not a perfect proxy for N_2O, it is not an unreasonable one, as in both these instances we are concerned with the poleward transport of a tropical source quantity.

Figure 8 compares the global meridional OGCM heat transport with estimates from *Macdonald and Wunsch* [1996], *Talley* [1984], and *Hastenrath* [1982]. As can be seen, the OGCM is in close agreement with the recent estimates of *Macdonald and Wunsch* [1996] but underestimates, by about a factor of 2 in the subtropics, the results of *Talley* [1984] in the Southern Hemisphere and *Hastenrath* [1982] in both hemispheres. Since these results deal with heat, it is not possible to directly evaluate the implications for meridional N_2O transport; if, however, N_2O transport from the tropics is also underestimated by a factor of 2, then an assumption of the doubling of the tropics to high-latitude N_2O transport reduces the total sea-air flux in the tropical 30°S to 30°N latitude band to 77% (OX1), 49% (OX.5), and 36% (OX.25) for the OX simulations. In comparison to the observational estimates of 41-42%, this suggests that if, in fact, the OGCM poleward transport is too low, then scenario OX.5 becomes more plausible, while OX1 still remains unlikely.

Finally, we note that although the above analysis indicates that relatively little of the N_2O formed in low-oxygen regions is transported meridionally to higher latitudes, the simulated distributions do display significant zonal transport in certain regions, particularly in the equatorial Pacific. *Suntharalingam* [1997] has examined the westward advection of N_2O from the low-oxygen waters of the eastern equatorial Pacific and compared the OX model distributions to the meridional transect (between longitudes 160°E-170°E) made in the western Pacific on the SAGA 2 cruise [*Butler et al.*, 1988; *Butler et al.*, 1989]. The observation-based section displays two "cores" of high-N_2O water straddling the equator within ±10° and at depths above 500 m. These cores of high N_2O in the western equatorial Pacific are reproduced in all the OX simulations, including OX1, which has no in situ N_2O production in this region, since local oxygen levels are higher than that required for activation of the low-oxygen N_2O source. Analysis of model transport indicates that these features predominantly result from westward advection of N_2O, both north and south of the equator, from the regions of intense production in the eastern equatorial Pacific. These "cores"

are separated at the equator by an eastward flowing tongue of low N_2O water transported from the western Pacific by the model's Equatorial Undercurrent [*Suntharalingam*, 1997]. In summary, the model simulations indicate that while meridional transport does not appear to play an important role, advection, in regions of strong zonal currents, can transport N_2O from the predominantly coastal low-oxygen waters to significant distances into the open ocean.

4. Summary and Conclusions

We have implemented models of enhanced N_2O production under low-oxygen conditions to evaluate the significance of such regions to the global oceanic N_2O distribution and sea-air flux. In comparison to a Base Case scenario, in which N_2O production depends on productivity alone, the effect of including a dependence on oxygen level in the N_2O source parameterization of this study is to shift the location of the source to the tropical latitudes (to the eastern boundaries of ocean basins, in general) and into the upper water column (to depths above 1000 m). The circulation in such regions is characterized by strong upwelling in the surface ocean. The majority of the N_2O formed in these zones, therefore, escapes directly to the atmosphere and is not subject to significant poleward transport. In the most extreme scenario, OX1, in which the entire source is formed in the low-latitude low-oxygen zones, over 87% of the source is vented to the atmosphere in the tropical latitude belt. A small fraction of the total source from these regions is transported poleward to the higher latitudes. The majority of this transport occurs in the upper ocean (depths above 1000 m), and relatively little is transported via the deep ocean.

Comparison with flux distributions based on observational data (shown in Figure 5) suggests that simulations OX.25, and to a lesser extent OX.5, which allocate 25% and 50%, respectively, of the total source to the low oxygen regions, come closest to matching the observations. We note, however, that the database underlying the observed estimates [*Weiss et al.*, 1992], is sparse in certain regions of potential significance to the global N_2O distribution; added coverage in the upwelling zone off Peru, the Arabian Sea (particularly during the southwest monsoon) and the Southern Ocean would help in better constraining this analysis.

We rely on the SAGA 2 data set of *Butler et al.* [1988] to evaluate the success of the model simulations at depth. The observed $\Delta N_2O/AOU$ ratios show a systematic decrease with depth below 500 m, suggesting a probable decrease in the rate of N_2O production with respect to oxygen consumption from remineralization at depth. The OX simulations of this study reproduce this aspect of the observations far more successfully than does the simple Base Case parameterization, since they give a greater emphasis to the low-oxygen source locations in the upper water column. Comparison of averaged profiles of $\Delta N_2O/AOU$ ratios (Figure 6) indicates that OX.25 provides the best fit to the data in the upper ocean where the majority of the N_2O formation occurs. This simulation appears to produce too much N_2O in the deep ocean, however, and a better fit to the data here is provided by OX.5, which produces two-thirds the level of deep N_2O as OX.25. It should be noted, however, that since the majority of total remineralization occurs in the upper water column, the nature of deep N_2O production has a relatively small impact on both the magnitude and spatial distribution of the global sea-air flux.

We note that certain problem characteristics of the OGCM and ocean biogeochemistry model have varying implications for our conclusions on N_2O transport out of the tropical region. The extents of the tropical low oxygen zones in the model are overestimated; hence a more realistic representation is likely to further constrain N_2O efflux to upwelling regions, leaving less N_2O available for transport to higher latitudes. On the other hand, if poleward transport in the OGCM is underestimated, as suggested by comparison with some heat transport estimates, this may result in an underestimate of poleward N_2O transport in the model.

In conclusion, analyses of the surface flux and depth distributions of the OX simulations suggest that the low-oxygen regions could provide a significant fraction of the global oceanic N_2O source; for example, simulations OX.25 and OX.5, which allocate a quarter and a half of the global source to these regions, respectively, succeed in matching certain characteristics of the observed distributions relatively well. Comparisons of modeled and observation-based flux distributions do not, however, support a scenario in which the majority of the global source originates in these regions (for example, close to 100%, as in the OX1 case). Surface observational data are, however, still sparse in some potentially significant oceanic areas, and increased coverage would aid in better constraining this analysis.

Acknowledgments. We thank J.H. Butler, L. Codispoti and R.J. Murnane for helpful discussions during the course of this study. We also gratefully acknowledge computer support from GFDL/NOAA through J. Mahlman. This work was supported by the U.S. Department of Energy under contract DEFG0290ER61052.

References

Anderson, L.A., and J.L. Sarmiento, Redfield ratios of remineralization determined by nutrient data analysis, *Global Biogeochem. Cycles, 8*, 65-80, 1994.

Anderson, L.A., and J.L. Sarmiento, Global ocean phosphate and oxygen simulations, *Global Biogeochem. Cycles, 9*, 621-636, 1995.

Bange, H.W., S. Rapsomanikis, and M.O. Andreae, Nitrous

oxide in coastal waters, *Global Biogeochem. Cycles, 10*, 197-207, 1996.

Benson, B.B., and D. Krause Jr., The concentration and fractionation of oxygen dissolved in freshwater and seawater in equilibrium with the atmosphere, *Limnol. Oceanogr., 29(3)*, 620-632, 1984.

Broecker, W.S., and T.H. Peng, Interhemispheric transport of carbon dioxide by ocean circulation, *Nature, 356*, 587-589, 1992.

Butler, J.H., J.W. Elkins, C.M. Brunson, K.B. Egan, T.M. Thompson, T.J. Conway, and B.D. Hall, Trace gases in and over the west Pacific and the east Indian Oceans during the El Nino Southern Oscillation event of 1987, *NOAA Data Rep. ERL ARL-16*, Natl. Oceanic and Atmos. Admin., Boulder, Colo., 1988.

Butler, J.H., J.W. Elkins, T.M. Thompson, and K.B. Egan, Tropospheric and dissolved N_2O of the west Pacific and east Indian Oceans during the El Nino Southern Oscillation event of 1987, *J. Geophys. Res., 94*, 14,865-14,877, 1989.

Cline, J.D., D.P. Wisegarver, and K. Kelly-Hansen, Nitrous oxide and vertical mixing in the equatorial Pacific during the 1982-1983 El Nino, *Deep Sea Res., 34*, 857-873, 1987.

Codispoti, L.A., and J. P. Christensen, Nitrification, denitrification, and nitrous oxide cycling in the eastern tropical South Pacific Ocean., *Mar. Chem., 16*, 277-300, 1985.

Codispoti, L.A., R.T. Barber, and G.E. Friedrich, Do the nitrogen transformations in the poleward undercurrent off Peru and Chile have a globally significant influence?, in *Poleward Flows Along Eastern Ocean Boundaries, Coastal Estuarine Stud.*, vol. 34, edited by S.J. Neshyba, C.N.K. Mooers, R.L. Smith, and R.T. Barber, pp.281-310, Springer-Verlag, New York, 1989.

Codispoti, L.A., J.W. Elkins, T. Yoshinari, G. Fredrich, C. Sakamoto, and T. Packard, On the nitrous oxide flux from productive regions that contain low oxygen waters, in *Oceanography of the Indian Ocean*, edited by B. Desai, pp.271-284, Oxford Univ. Press, New York, 1992.

Cohen, Y., and L.I. Gordon, Nitrous oxide in the oxygen minima of the eastern tropical North Pacific: Evidence for its consumption during nitrification and possible mechanism for its production, *Deep Sea Res., 25*, 509-524, 1978.

Cohen, Y., and L.I. Gordon, Nitrous oxide production in the ocean, *J. Geophys. Res., 84*, 347-353, 1979.

Elkins, J.W., S.C. Wofsy, M.B. McElroy, C.E. Kolb, and W.A. Kaplan, Aquatic sources and sinks for nitrous oxide, *Nature, 275*, 602-606, 1978.

Esbensen, S.K., and Y. Kushnir, The heat budget of the global ocean: An atlas based on estimates from surface marine observations, *Rep. 29*, Clim. Res. Inst., Oreg. State Univ., Corvallis, 1981.

Goreau, T., W.A. Kaplan, S.C. Wofsy, M.B. McElroy, F.W. Valois, and S.W. Watson, Production of NO_2^- and N_2O by nitrifying bacteria at reduced concentrations of oxygen, *Appl. Environ. Microbiol., 40*, 526-532, 1980.

Hahn, J., The North Atlantic Ocean as a source of atmospheric N_2O, *Tellus, 26*, 160-168, 1974.

Hashimoto, L.K., W.A. Kaplan, S.C. Wofsy, and M.B. McElroy, Transformations of fixed nitrogen and N_2O in the Cariaco Trench, *Deep Sea Res., 30*, 575-590, 1983.

Hastenrath, S.J., On meridional heat transports in the world ocean, *J. Phys. Oceanogr., 12*, 922-927, 1982.

Hellerman, S., and M. Rosenstein, Normal monthly wind stress over the world ocean with error estimates, *J. Phys. Oceanogr., 13*, 1093-1104, 1983.

Horrigan, S.G., A.F. Carlucci, and P.M. Williams, Light inhibition of nitrification in sea-surface films, *J. Mar. Res., 39*, 557-565, 1981.

Houghton, J.T., G.J. Jenkins, and J.J. Ephraums, *Climate Change: The IPCC Scientific Assessment*, Cambridge Univ. Press, New York, 1990.

Jorgensen, K.S., H.B. Jensen, and J. Sorensesn, Nitrous oxide production from nitrification and denitrification in marine sediment at low oxygen concentrations, *Can. J. Microbiol., 30*, 1073-1078, 1984.

Junge, C., B. Bockholt, K. Schutz, and R. Beck, N_2O measurements in air and sea water over the Atlantic, *"Meteor" Forschungsergeb., Reihe B, 6*, 1-11, 1971.

Keeling, R.F., and T.H. Peng, Transport of heat, CO_2 and O_2 by the Atlantic's thermohaline circulation, *Philos. Trans. R. Soc. London, 348*, 133-142, 1995.

Law, C.S., and N.J.P. Owens, Significant flux of atmospheric nitrous oxide from the northwest Indian Ocean, *Nature, 346*, 826-828, 1990.

Levitus, S., *Climatological Atlas of the World Ocean, NOAA Prof. Pap. 13*, Natl. Oceanic and Atmos. Admin., Silver Spring, Md., 1982.

Levitus, S., M.E. Conkright, and T.P. Boyer, *World Ocean Atlas*, Natl. Oceanic and Atmos. Admin., Silver Spring, Md., 1994.

Macdonald, A.M., and C. Wunsch, An estimate of global ocean circulation and heat fluxes, *Nature, 382*, 436-439, 1996.

Murnane, R., J.L. Sarmiento, and C. Le Quere, Spatial distribution of air-sea CO_2 fluxes and the interhemispheric transport of carbon by the ocean, *Global Biogeochem. Cycles, 13*, 287-306, 1999.

Najjar, R.G., Simulations of the phosphorus and oxygen cycles in the world ocean using a general circulation model, Ph.D. thesis, Princeton Univ., Princeton, N.J., 1990.

Najjar, R.G., J. L. Sarmiento, and J. R. Toggweiler, Downward transport and fate of organic matter in the oceans: Simulations with a general circulation model, *Global Biogeochem. Cycles, 6*, 45-76, 1992.

Naqvi, S.W.A., and R.J. Noronha, Nitrous oxide in the Arabian Sea, *Deep Sea Res., Part A, 38*, 871-890, 1991.

Naqvi, S.W.A., T. Yoshinari, M.A. Altabet, D.A. Jayakumar, P.V. Narvekar, and L.A. Codispoti, Variability of redox conditions in the Intermediate Waters of the Arabian Sea: Effect on nitrous oxide cycling, *Eos Trans. AGU, 76(3)*, Ocean Sci. Meet. Suppl., OS2, 1996.

Nevison, C.D., R.F. Weiss, and D.J. Erickson III, Global oceanic nitrous oxide emissions, *J. Geophys. Res., 100*, 15,809-15,820, 1995.

Pacanowski, R., K. Dixon and A. Rosati, The GFDL Modular Ocean Model Users' Guide, *GFDL Ocean Group Tech. Rep. 2*, Geophys. Fluid Dyn. Lab., Natl. Oceanic and Atmos. Admin., Princeton, N.J., 1993.

Prosperie, L.F., L.A. Codispoti, S.W.A. Naqvi, J. Aftab, D. Masten, R. Patrick, and R. Williams, Oxygen deficient (suboxic) conditions in the Arabian Sea, *Eos Trans. AGU, 76(3)*, Ocean Sci. Meet. Suppl., OS3, 1996.

Rao, C.K., S.W.A. Naqvi, M.D. Kumar, S.J.D. Varaprasad, D.A. Jayakumar, M.D. George, and S.Y.S. Singbal, Hydrochemistry of the Bay of Bengal: Possible reasons for a different water-column cycling of carbon and nitrogen from the Arabian Sea, *Mar. Chem., 47*, 279-290, 1994.

Sarmiento, J.L., R. Murnane, and C. Le Quere, Air-sea CO_2 transfer and the carbon budget of the North Atlantic, *Philos. Trans. R. Soc. London, Ser.B, 348*, 211-219, 1995.

Suntharalingam, P., Modeling the global oceanic nitrous ox-

ide distribution, Ph.D. thesis, Princeton Univ., Princeton, N.J., 1997.

Suntharalingam, P., and J.L. Sarmiento, Factors governing the global oceanic nitrous oxide distribution: simulations with an ocean general circulation model, *Global Biogeochem. Cycles, 14*, 429-454, 2000.

Talley, L.J., Meridional heat transport in the Pacific Ocean, *J. Phys. Oceanogr., 14*, 231-241, 1984.

Toggweiler, J.R., K. Dixon, and K. Bryan, Simulations of radiocarbon in a coarse resolution world ocean model, 1: Steady state distributions, *J. Geophys. Res., 94*, 8217-8242, 1989a.

Toggweiler, J.R., K. Dixon and K. Bryan, Simulations of radiocarbon in a coarse resolution world ocean model 2: Distributions of bomb-produced ^{14}C , *J. Geophys. Res., 94*, 8243-8264, 1989b.

Toggweiler, J.R., K. Dixon and W. Broecker, The Peru upwelling and the ventilations of the South Pacific thermocline, *J. Geophys. Res., 96*, C11, 20,467-20,497, 1991.

Toggweiler, J.R., and B. Samuels, New radiocarbon constraints on the upwelling of abyssal water to the ocean's surface, in *The Global Carbon Cycle, NATO ASI Ser., Ser. I*, vol. 15, 333-366, Springer-Verlag, New York, 1993.

Tschuyia, M., *Upper Waters of the Intertropical Pacific Ocean, Johns Hopkins Oceanogr. Stud.*, vol. 4, Johns Hopkins Univ. Press, Baltimore, 1968.

Wanninkhof, R., Relationship between wind speed and gas exchange over the ocean, *J. Geophys. Res., 97*, 7373-7382, 1992.

Ward, B.B., H.E. Glover, and F. Lipschultz, Chemoautotrophic activity and nitrification in the oxygen minimum zone off Peru, *Deep Sea Res., 36*, 1031-1051, 1989.

Weiss, R.F., F. A. Van Woy, and P. K. Salameh, Surface water and atmospheric carbon dioxide and nitrous oxide observations by shipboard automated gas chromatography: results from expeditions between 1977 and 1990, *Scripps Inst. of Oceanogr. Ref. 92-11*, Scripps Inst. of Oceanogr., San Diego, Calif., 1992.

Wyrtki, K., The oxygen minima in relation to ocean circulation, *Deep Sea Res., 9*, 11-23, 1962.

Wyrtki, K., An estimate of equatorial upwelling in the Pacific, *J. Phys. Oceanogr., 11*, 1205-1214, 1981.

Yoshida, T., and M. Alexander, Nitrous oxide formation by *Nitrosomonas europae* and heterotrophic microorganisms, *Soil Sci. Soc. Am. Proc., 34*, 880-882, 1970.

Yoshinari, T., Nitrous oxide in the sea, *Mar. Chem., 4*, 189-202, 1976.

P. Suntharalingam, Department of Earth and Planetary Sciences, Harvard University, Pierce Hall, 29 Oxford Street, Cambridge, Massachusetts 02138. (e-mail: pns@sol.harvard.edu)

J.L. Sarmiento, Program in Atmospheric and Oceanic Sciences, P.O. Box CN710, Sayre Hall, Princeton University, Princeton, New Jersey 08544-0710.

J.R. Toggweiler, Geophysical Fluid Dynamics Laboratory/NOAA, P.O. Box 308, Princeton, New Jersey 08542-0308.

(Received August 24, 1998; revised September 17, 1999; accepted September 22, 1999.)